Nonlinear Damping in Micro -Speakers

Wolfgang Klippel

The mechanical and acoustical losses considered in the lumped parameter modeling of electro-dynamical transducers may become a dominant source of nonlinear distortion in micro-speakers, tweeters, headphones and some horn compression drivers where the total quality factor Q_{ts} is not dominated by the electrical damping realized by a high force factor Bl and a low voice resistance R_e. This paper presents a nonlinear model describing the generation of the distortion and a new dynamic measurement technique for identifying the nonlinear resistance $R_{ms}(v)$ as a function of voice coil velocity v. The theory and the identification technique are verified by comparing distortion and other nonlinear symptoms measured on micro-speakers as used in cellular phones with the corresponding behavior predicted by the nonlinear model.

1   Introduction

Micro-speakers play an important role in personal audio devices such as cellular phones, laptops and other portable systems which require small transducers generating sufficient sound pressure in the audio band at high efficiency.
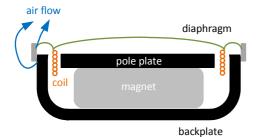

Figure 1: Sectional view of a micro-speaker

Most of the currently used micro-speakers use the electro-dynamical principle as illustrated in Figure 1. Micro-speakers are used without additional subwoofers and have to generate the required volume velocity with a relatively high peak displacement because the effective radiation area S_d is limited. Thus micro-speakers are operated in the nonlinear working range exploiting all available resources up to the physical limits. Optimal design of the mechanical suspension (which uses the diaphragm itself) and the motor structure requires insight into nonlinear and thermal mechanisms. The nonlinear model [1] developed for woofers, tweeters, headphones, compression drivers and other electro-dynamical transducers cannot explain some particularities found in micro-speakers. This paper develops an extended model which will be verified by practical measurements.
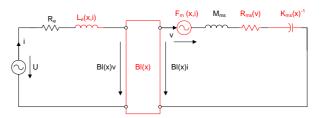

Figure 2: Equivalent circuit of the electro-acoustical transducer using lumped elements with nonlinear parameters

2   Extended Transducer Model

At low frequencies where the wave length is large in comparison to the physical dimensions of the transducer the electro-dynamical transducer can be modeled by lumped elements [2] as shown in the Figure 2 with linear and nonlinear parameters:

R_e	Electrical resistance of the voice coil,
$L_e(x,i)$	Electrical inductance of the voice coil depending on voice coil displacement x and input current i,
$Bl(x)$	Force factor of the electro-dynamical motor depending on voice coil displacement x,
$F_m(x,i) = -\dfrac{i^2}{2}\dfrac{dL_e(x)}{dx}$	Reluctance force caused by displacement varying inductance $L_e(x)$,
$K_{ms}(x)=C_{ms}(x)^{-1}$	Stiffness (inverse of the compliance) of the mechanical suspension depending on displacement x,
M_{ms}	Moving mass of all mechanical parts including air load,
$R_{ms}(v)$	Mechanical and acoustical losses varying with voice coil velocity v.

The linear elements have constant parameters and the nonlinear elements are functions of voice coil displacement x, current i and voice coil velocity v.

The force factor $Bl(x)$ and stiffness $K_{ms}(x)$ are dominant nonlinearities in all electro-dynamical transducers because those parameters are closely related to the height of the voice coil, the gap depth and the number and size of the corrugation rolls in the mechanical suspensions. The nonlinearity of the voice coil inductance $L_e(x,i)$ plays an important role in woofers and subwoofers [3] but can be neglected in micro-speakers.

The effect of the transducer nonlinearities can be investigated by the nonlinear differential equation

$$K_{ms}(x)x + \left(R_{ms}(v) + \frac{Bl(x)^2}{R_e}\right)v + M_{ms}\frac{dv}{dt} . \qquad (1)$$
$$= \frac{Bl(x)}{R_e}\left(u(t) - \frac{d(L_e(i,x)i)}{dt}\right) + \frac{i^2}{2}\frac{dL_e(x)}{dx}$$

corresponding to the sum of forces in the mesh on the right-hand side of the equivalent circuit in Figure 2. The $K_{ms}(x)$-nonlinearity generates a nonlinear restoring force $K_{ms}(x)x$ which causes multiplications of displacement x with a nonlinear function of x. The $Bl(x)$-nonlinearity occurs as a multiplicative factor causing a variation of the electro-dynamical excitation force on the right-hand side of Eq. (1) and a nonlinear damping force $Bl(x)^2 v/R_e$ on the left-hand side. The nonlinear inductance $L_e(x,i)$ also has two effects such as self-induction in the electrical mesh in Figure 2 and the reluctance force $F_m(x,i)$ corresponding with an electro-magnetic excitation if the local derivative of the inductance is not negligible. The $R_{ms}(v)$-nonlinearity introduced in the new extended model Figure 2 generates a second nonlinear damping force $R_{ms}(v)v$ which has been neglected in woofers and subwoofers so far. This nonlinearity becomes important in micro-speakers, head-phones and some other transducers because the electrical damping generated by a high force factor Bl becomes smaller than the mechanical or acoustical damping and the total loss factor Q_{ts} is dominated by the mechanical Q_{ms}.

2.1 Signal Flow Chart

Considering only the effect of the $R_{ms}(v)$-nonlinearity and connecting the transducer to an amplifier with a high impedance output (behaving as a current source) the generation of the nonlinear distortion in the voice coil velocity v can be described by the integro-differential equation

$$v = L^{-1}\left\{\frac{s}{K_{ms} + R_{ms}(0)s + M_{ms}s^2}\right\} * \left(Bli - (R_{ms}(v) - R_{ms}(0))v\right) \qquad (2)$$

using the convolution symbol *, the Laplace operator s and the inverse Laplace transformation $L^{-1}\{\}$. To the linear excitation force Bli a nonlinear distortion signal $(R_{ms}(v) - R_{ms}(0))v$ is added and generates a feedback loop as illustrated in the signal flow chart in
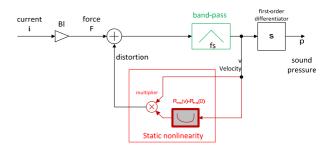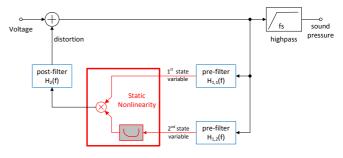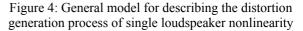   Figure 3.

Figure 3: Signal flow chart describing the effect of the nonlinear resistance $R_{ms}(v)$ in a transducer under current supply.

The band-pass filter generates the velocity v supplied to a static nonlinearity and attenuates components below and above the fundamental resonance f_s. The distortion generated at the output of the static nonlinearity is transferred via the same band-pass and a first-order differentiator into the sound pressure output signal $p(t)$.

Figure 4: General model for describing the distortion generation process of single loudspeaker nonlinearity

The signal flow chart of the transducer with $R_{ms}(v)$-nonlinearity in Figure 3 has the same topology as the general model in Figure 4 used for modeling single effects of other transducer nonlinearities. The general model comprises a linear high-pass representing the loudspeaker in the small signal domain, a static nonlinearity and linear pre-filters having a transfer function $H_{1,1}(f)$, $H_{1,2}(f)$, and a post filter $H_2(f)$ having properties as listed in Table 1.

Table 1: Properties of the pre- and post-filter of the dominant transducer nonlinearities and in parenthesis the state signals multiplied by the nonlinear processing.

Non-linearity	Pre-filter $H_{1,1}(f)$ (output)	Pre-filter $H_{1,2}(f)$ (output)	Post-filter $H_2(f)$
Stiffness $K_{ms}(x)$	Low-pass (displacement)	Low-pass (displacement)	1
Force factor $Bl(x)$	Band-stop (current i)	Low-pass (displacement)	1
	Band-pass (velocity)	Low-pass (displacement)	1
Inductance $L_e(x)$	Band-stop (current i)	Low-pass (displacement)	differentiator
	Band-stop (current i)	Low-pass (displacement)	1
Inductance $L_e(i)$	Band-stop (current)	Band-stop (current)	differentiator
Mechanical resistance $R_{ms}(v)$	Band-pass (velocity)	Band-pass (velocity)	1

The nonlinear stiffness $K_{ms}(x)$ requires a low-pass for both pre-filters $H_{1,1}(f)$ and $H_{1,2}(f)$ to generate the voice coil displacement x multiplied in the static nonlinearity. There is no additional post-filter $H_2(t)$ required between the multiplier output and the input of the high-pass. The first nonlinear effect of the force factor $Bl(x)$ requires a band-stop filter and a low-pass to generate the electrical current i and the displacement x, respectively. The nonlinear damping also generated by $Bl(x)$ requires a band-pass instead of the band-stop filter to generate the velocity v multiplied with a function of the voice coil displacement x. The nonlinear inductance $L_e(x)$ also has two nonlinear effects which require the band-stop and a low-pass filter to generate the current i and displacement x, respectively, in the pre-filters. However, the self-induction causes an additional differentiator in the post-filter which corresponds to the differentiation of the magnetic flux in Eq. 1. The $L_e(i)$-nonlinearity requires a multiplication of the current i which can be generated by a band-stop filter and a following differentiation in the post filter $H_2(f)$. The mechanical resistance $R_{ms}(v)$ introduced in the new extended model performs a multiplication of the velocity v provided by a band-pass filter and additional shaping in the post-filter $H_2(f)$.

The properties of the linear filters $H_{1,1}(f)$, $H_{1,2}(f)$ and $H_2(f)$ which are different for each nonlinearity determine the dynamic behavior of the overall system and the spectral properties of the distortion components.

3 Parameter Identification

To apply the theory to a particular transducer the free parameters of the model have to be determined by using static, incremental or full dynamic measurment techniques as defined in the IEC standard [4]. The dynamic method as illustrated in Figure 5 also uses the nonlinear model which is connected in parallel to the transducer and supplied by an arbitrary a.c. signal $u(t)$ such as noise, music or other ordinary audio signals.
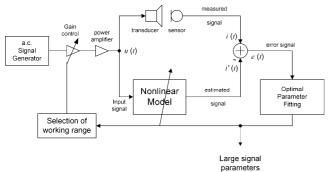
Figure 5: Dynamical measurement of transducer parameters by adaptive modeling of the input current

The optimal transducer parameters are determined by monitoring a state variable of the transducer such as the electrical input current $i(t)$ and by comparing the measured signal with the estimated current $i'(t)$ at the output of the model and by minimizing the error signal $e(t) = i(t) - i'(t)$ in a quadratic cost function [5].
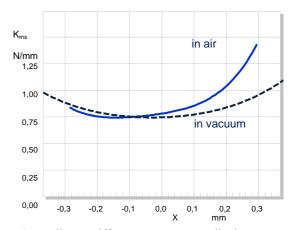
Figure 6: Nonlinear stiffness $K_{ms}(x)$ versus displacement x of a micro-speaker measured in air (solid curve) and in vacuum (dashed curve)
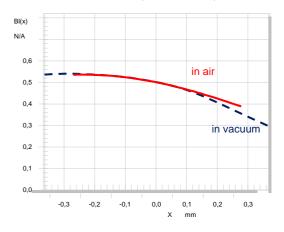
Figure 7: Nonlinear force factor $Bl(x)$ versus displacement x of a micro-speaker measured in air (solid curve) and in vacuum (dashed curve)
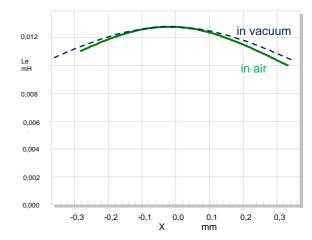
Figure 8: Nonlinear inductance $L_e(x)$ versus displacement x of a micro-speaker measured in air (solid curve) and in vacuum (dashed curve)
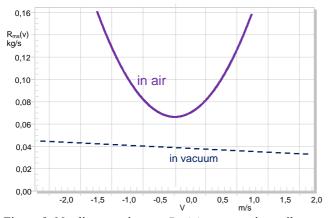
Figure 9: Nonlinear resistance $R_{ms}(v)$ versus voice coil velocity v of a micro-speaker measured in air (solid curve) and in vacuum (dashed curve)

This technique has been applied to a small micro-speaker used as an example throughout this paper. Figure 6 shows the nonlinear stiffness $K_{ms}(x)$ of this speaker operated in free air and in vacuum. The vacuum measurement reveals the properties of the mechanical suspension without the influence of air cavities in the transducer causing a distinct asymmetry in the $K_{ms}(x)$ curve. Both $Bl(x)$-curves measured in air and vacuum in Figure 7 show an offset of $x_{off}\approx$ 0.25 mm in the rest position of the voice coil. The air also has no significant influence on the $L_e(x)$-nonlinearity in Figure 8 but causes large difference in the measured $R_{ms}(v)$-curve in Figure 9. Thus more than 50 % of the mechanical resistance $R_{ms}(v)$ is caused by the viscous air flow in the gap and at leaks in the micro-speaker. The pure mechanical resistance is almost constant while the air causes a symmetrical increase of the resistance independent of the direction of the air flow.

Table 2: Peak value of the nonlinear distortion in the simulated sound pressure output signal generated by each nonlinearity

DISTORTION caused by	AIR	VACUUM
$K_{ms}(x)$	28%	36 %
$Bl(x)$	20 %	17 %
$L_e(x)$	2%	2%
$R_{ms}(v)$	45%	6%

The model with the identified parameters makes it possible to measure the peak value of nonlinear distortion generated by each nonlinearity referred to the peak value of the total sound pressure output. Table 2 reveals that the $R_{ms}(v)$-nonlinearity generates the dominant distortion in the sound pressure output if the transducer is operated in free air and if excited by a broad-band noise similar to an ordinary audio signal. The distortion generated by $R_{ms}(v)$ almost vanishes and the stiffness $K_{ms}(x)$ becomes the dominant source of distortion if the micro-speaker is operated in vacuum. The distortion generated by the $L_e(x)$-nonlinearity is almost negligible because the impedance generated by the inductance is much smaller than the dc-resistance of the voice coil.

4   Nonlinear Symptoms

A transducer operated at high amplitudes generates nonlinear effects which are not found at small amplitudes [6]. For example, the detection of harmonics and other spectral components which are not supplied by the stimulus indicates nonlinearities somewhere in the system. However, the a-priori knowledge provided by the physical modelling simplifies the interpretation of the large signal behaviour and is the basis for a root cause analysis.

In this chapter the nonlinear symptoms are predicted by using the extended model and the nonlinear parameters measured on the particular micro-speaker. Comparing the predicted symptoms with the results of a direct measurement is the basis for verifying the model and the parameter identification technique [7]. Furthermore, the effect of each transducer non-linearity is investigated separately by generating virtual design choices where only one nonlinearity is considered and all the other parameters are assumed as linear.

4.1   Displacement

The most fundamental nonlinear symptom is the compression of the voice coil peak displacement at high amplitudes [10]. This limits not only the acoustical output at low frequencies but also produces less distortion by $Bl(x)$, $K_{ms}(x)$ and other nonlinearities which depend on displacement x.
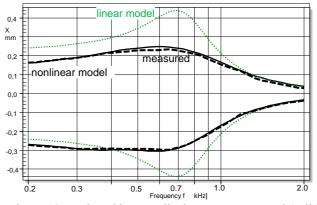

Figure 10: Peak and bottom displacement measured (solid line) and predicted by using a linear model (dotted curve) and a nonlinear model (dashed curve)

Figure 10 shows good agreement between the measured and predicted peak displacement for a sinusoidal tone with 2 V rms input voltage using the nonlinear parameters of the micro-speaker discussed in this paper. A linear model neglecting the inherent nonlinearities would produce a much higher peak displacement at 700 Hz.
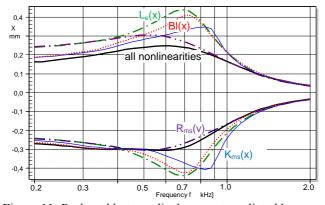
Figure 11: Peak and bottom displacement predicted by using all nonlinear parameters (solid line) and by considering each separated nonlinear cause

Figure 11 shows the peak displacement predicted by the model considering one selected nonlinearity. The $L_e(x)$-curve in this example is a weak nonlinearity and produces almost the same peak displacement as the linear system. Neither the force factor $Bl(x)$ nor the stiffness $K_{ms}(x)$ can explain the high damping of the resonance peak at 700 Hz. However, the extended model considering the nonlinear resistance $R_{ms}(v)$ generates this kind of amplitude compression at resonance but behaves like the linear system at very low frequencies.
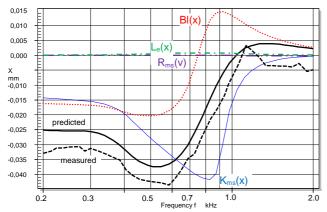

Figure 12: Measured (dashed line) and predicted (solid line) dc displacement versus frequency f and the contribution of each nonlinearity

Figure 10 already revealed a difference in the peak and bottom value of the measured and simulated displacement corresponding with the dc-displacement depicted in Figure 12. In consideration of visco-elastic uncertainties in the suspension material at low frequencies ("creep" effect [8]) there is a good agreement between laser measurement and model considering all nonlinear parameters. The negative dc-displacement of 35 μm at the resonance frequency f_s= 700 Hz is caused by $K_{ms}(x)$. At lower frequencies $Bl(x)$ and $K_{ms}(x)$ contribute the same amount to the total dc-displacement. The $Bl(x)$-nonlinearity generates a positive dc-displacement above 900 Hz which increases the voice coil offset which is almost compensated by the stiffness nonlinearity. The $L_e(x)$ and $R_{ms}(v)$ nonlinearity does not significantly contribute to the total dc-displacement because the curve shape of both nonlinearities is almost symmetrical.
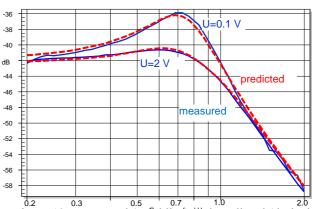

Figure 13: Measured (solid line) and predicted (dashed line) amplitude ratio of the fundamental component of voice coil displacement x and input voltage U in the small and large signal domain

Figure 13 reveals a compression of 6 dB of the fundamental component at 700 Hz by increasing the voltage at the terminals from 0.1 to 2 V. This corresponds to a reduction of the total quality factor from about 2 in the small signal domain to 1 in the large signal domain.
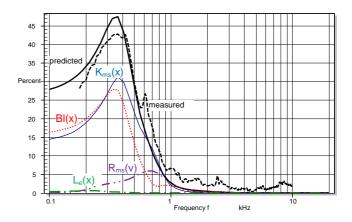

Figure 14: Total harmonic distortion in percent measured in the sound pressure output (dashed line) and simulated by nonlinear modeling using all nonlinearities (solid line) and each separated nonlinearity

4.2 Harmonic Distortion

The total harmonic distortion measured with a single-tone stimulus with varying frequency f is the most popular measurement of nonlinear symptoms [9]. Figure 14 shows the measured distortion with the predicted response using all nonlinearities and the contribution of each nonlinearity. At frequencies below resonance the force factor $Bl(x)$ and stiffness $K_{ms}(x)$ are the dominant causes of the distortion. The relative distortion value exceeds here 40% because the absolute amplitude of distortion is referred to the total rms value of the sound pressure output which decreases in this frequency range by a slope of 12 dB per octave caused by the high-pass in Figure 4.

An interesting alternative is the measurement of the equivalent input distortion [11] which describes the ratio of the distortion at the output of the nonlinear feedback loop and second input of the adder Figure 4 referred to the output signal of the adder.
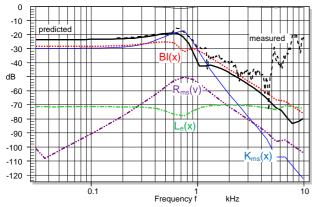
Figure 15: Measured (dashed line) and predicted (solid line) 2nd-order equivalent harmonic input distortion versus frequency f and the contribution of each nonlinearity

Figure 15 shows a good agreement between the measured and predicted 2nd-order equivalent harmonic input distortion at low frequencies. In this frequency range the input distortion is about 8 % of the input signal which corresponds with 80mV for a sinusoidal input of 1 V rms. The discrepancy above 6 kHz is caused by measurement noise transferred into equivalent input distortion erroneously. Clearly the asymmetrical curve shape of $Bl(x)$ and $K_{ms}(x)$ accounts for 2nd-order distortion below f_s. At high frequencies the distortion is generated by $Bl(x)$ only and by nonlinear vibration of the break-up modes.
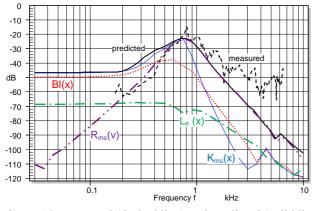

Figure 16: Measured (dashed line) and predicted (solid line) 3rd-order equivalent harmonic input distortion versus frequency f and the contribution of each nonlinearity

Figure 16 reveals the nonlinear resistance $R_{ms}(v)$ as the dominant source of the 3rd-order distortion at resonance frequency and above. Contrary to the $Bl(x)$ and $K_{ms}(x)$ distortion the distortion generated by $R_{ms}(v)$ depends on the velocity and falls to lower and higher frequencies with the distance to the resonance frequency f_s=700 Hz.
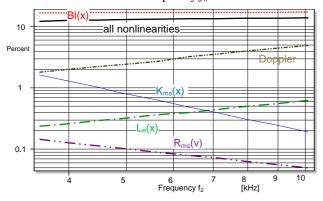

Figure 17: 2nd-order intermodulation distortion versus frequency f_2 generated by a two-tone stimulus (with $f_2 > f_1$=400 Hz) considering all nonlinearities (thick solid line) and only one selected nonlinearity in the modeling

4.3 Intermodulation Distortion

The measurement of the intermodulation distortion (IMD) reveals the interaction with the two state variables multiplied in the static nonlinearity depicted in Figure 4. The frequency response of the intermodulation products directly corresponds to the properties of the pre-filters $H_{1,1}(f)$ and $H_{1,2}(f)$ and the post filter $H_2(f)$. There are many way of measuring intermodulation distortion defined in various standards. The interpretation of the IMD frequency responses can be simplified by using a two-tone stimulus where the frequency of one tone is varied and the frequency of the other tone is constant.

For the particular micro-speaker used as example the 2nd-order IMD in Figure 17 is almost independent of the frequency f_1 of the first tone above 15 %. Only the IMD generated by the force factor $Bl(x)$ has a similar curve shape and is the dominant source of this distortion component generated by the fundamental component at f_1 in electrical current and the fundamental displacement of the second tone at f_2=400 Hz. The nonlinear model considering only the $Bl(x)$-nonlinearity generates a slightly higher value of IMD than the complete modeling because the $K_{ms}(x)$ and the other nonlinearities cause an additional amplitude compression of the fundamental displacement as discussed in connection with Figure 11 before. Although the $K_{ms}(x)$ generates significant 2nd-order harmonics of f_1 as shown in Figure 16 the IMD fall with the displacement generated by the second tone at a slope of 12 dB per octave to higher frequencies f_2. However, the IMD generated by $L_e(x)$- and Doppler-distortion rise by 6 dB per octave to higher frequencies f_1 because the output of the static nonlinearity is differentiated in the post filter $H_2(f)$.
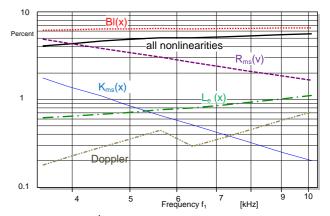

Figure 18: 3rd-order intermodulation distortion versus frequency f_2 generated by a two-tone stimulus (with $f_2 > f_1$=400 Hz) considering all nonlinearities (thick solid line) and only one selected nonlinearity in the modeling

The 3rd-order intermodulation distortion in Figure 18 is dominated by the $Bl(x)$- and $R_{ms}(v)$-nonlinearity. While the IMD generated by $Bl(x)$ only is almost constant versus frequency the falling slope of the $R_{ms}(v)$ causes a destructive interference in the total IMD at lower frequencies f_1.
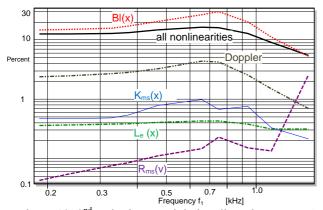
Figure 19: 2nd-order intermodulation distortion versus f_1 generated by a two-tone stimulus (with $f_1 < f_2 = 6$ kHz) considering all nonlinearities (thick solid line) and only one selected nonlinearity in the modeling

An alternative measurement of IMD distortion performs a variation of the low frequency tone f_1 while keeping the high-frequency tone f_2 at a fixed frequency. Figure 19 shows the 2nd-order IMD which is dominated by the $Bl(x)$-nonlinearity. For frequencies $f_1 > f_s = 700$ Hz the IMD distortion falls with the voice coil displacement generated by the first tone.
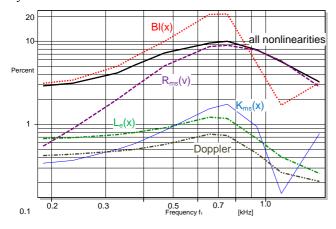

Figure 20: 3rd-order intermodulation distortion versus f_1 generated by a two-tone stimulus (with $f_1 < f_2 = 6$ kHz) considering all nonlinearities (thick solid line) and only one selected nonlinearity in the modeling

Figure 20 reveals the $Bl(x)$ and $R_{ms}(v)$ as the dominant cause of the 3rd-order intermodulation distortion at resonance frequency. Again the contribution of the force factor $Bl(x)$ is overestimated because the amplitude compression caused by $K_{ms}(x)$ is not considered.

5 Conclusion

The dependency of the mechanical resistance $R_{ms}(v)$ on voice velocity v is a dominant nonlinearity in micro-speakers and other transducers which have a relatively high resonance frequency f_s, a relatively small force factor Bl and a total quality factor Q_{ts} dominated by the mechanical losses. This nonlinearity can be neglected in woofers using a strong motor with a high value of the force factor Bl, a small dc resistance R_e and being operated by a voltage supply where the electrical damping dominates the mechanical damping. The $R_{ms}(v)$-nonlinearity causes at resonance frequency a significant increase of the mechanical damping causing a nonlinear amplitude compression of the fundamental and generating significant harmonic and intermodulation distortion. The extended transducer presented here has been verified on a variety of micro-speakers by identifying the curve shape of the nonlinearities and by comparing the predicted and measured large signal behavior.

There are strong indications that the nonlinear variation of R_{ms}-nonlinearity is not caused by the mechanical vibration of the diaphragm or other mechanical elements because the nonlinearity has always vanished when the micro-speaker was operated in vacuum. Further research is required to understand the physical details of the distortion mechanisms which is closely related to air flow and might be initiated by air turbulences in the gap and leakages of the diaphragm.

References

[1] W. Klippel, Tutorial: "Loudspeaker Nonlinearities - Causes, Parameters, Symptoms," J. Audio Eng. Society 54, No. 10 pp. 907-939 (2006 Oct.).

[2] A. J. M. Kaizer, "Modeling of the Nonlinear Response of an Electrodynamic Loudspeaker by a Volterra Series Expansion," J. Audio Eng. Soc., vol. 35, pp. 421-433 (1987 June).

[3] M. Dodd, et. al., "Voice Coil Impedance as a Function of Frequency and Displacement" presented at the 117th Convention of the Audio Eng. Soc. , 2004 October 28–31, San Francisco, CA, USA.

[4] "Sound system equipment - Electroacoustical transducers - Measurement of large signal parameters", International Electrotechnical Commission, PAS 62458 IEC:2006(E).

[5] W. Klippel, "Measurement of Large-Signal Parameters of Electrodynamic Transducer," presented at the 107th Convention of the Audio Engineering Society, New York, September 24-27, 1999, preprint 5008.

[6] M. Knudsen, et. al., "Determination of Loudspeaker Driver Parameters Using a System Identification Technique," ," J. Audio Eng. Soc. vol. 37, No. 9.

[7] D. Clark, "Precision Measurement of Loudspeaker Parameters," J. Audio Eng. Soc. vol. 45, pp. 129 – 140, (1997 March).

[8] M.H. Knudsen et. al., "Low-Frequency Loudspeaker Models that Include Suspension Creep," J. Audio Eng. Soc., vol. 41, pp. 3-18, (Jan./Feb. 1993).

[9] "Sound System Equipment. Part 5: Loudspeakers," IEC Publication 60268-5.

[10] W. Klippel, "Assessment of Voice-Coil Peak Displacement Xmax," J. Audio Eng. Society 51, No. 5, pp. 307 - 323 (2003 May).

[11] W. Klippel, "Equivalent Input Distortion," J. Audio Eng. Society 52, No. 9 pp. 931-947 (2004 Sept.).